Basin-Boundary Crossing Transitions in the Bistable Belousov−Zhabotinsky Reaction

F. Ali, P. Strizhak,† and M. Menzinger*

Department of Chemistry, University of Toronto, Toronto, Ontario M5S.3H6, Canada

Received: April 30, 1997; In Final Form: June 23, 1997[⊗]

Basin-boundary crossing transitions, induced by large and sudden perturbations of a dynamical variable or of a control parameter, are reported in the bistable Belousov−Zhabotinsky reaction in a continuously stirred tank reactor. We provide a geometrical interpretation of these transitions by constructing a response diagram in (2 + 1)-dimensional (phase + parameter) space, that displays the geometry of the basin boundary together with the customary parameter dependence of steady states. The observed ease of basin-boundary crossing arises from the proximity of the basin boundary and the manifold of initial steady states. This is shown to be caused by the flow in phase space that is peculiar to stiff systems with fast and slow variables. On the mechanistic level, the elementary step is identified that accounts for the divergence of trajectories from the basin boundary.

1. Introduction

Many dynamical systems in physics, chemistry, biology, and engineering are bistable. The nature of the system frequently requires that it be maintained in one of the coexisting states (e.g. the live or productive state) and that inadvertent transitions to the competing attractor be avoided. Therefore, to be able to safeguard the integrity of such systems, it is essential to know the critical domains in parameter and phase spaces where transitions occur.[1]

In bistable systems, transitions take place either through saddle-node bifurcations at critical values of the control parameter(s) or through the crossing of a basin boundary into the basin of a competing attractor. While the critical parameter values of saddle-node transitions are usually easy to determine, basin boundaries are less readily accessible, and their locations are generally unknown. In the course of studies of chemical bistability in the chlorite/iodide system we encountered such basin-boundary crossings (BBC) that seemed initially surprising until they were associated with the BBC mechanism. We present here an experimental study of BBC in the Belousov−Zhabotinsky (BZ) reaction together with numerical simulations and kinetic interpretations.

Bistable systems are often characterized by a steady state bifurcation diagram similar to the one shown schematically in Figure 1, which represents the local, adiabatic response to small parameter changes. On the other hand, phase portraits and basin boundaries in phase space, which describe the global response to large, nonadiabatic perturbations, are less readily available from experiments[2] and are often considered only qualitatively[3,4] but may be computed for model systems.[1,5,6] It would be valuable to combine the representation of steady states of the response diagram with the basin boundaries to obtain a quantitative tool for interpreting and predicting both types of transitions.

For systems with a single dynamical variable, the bifurcation diagram shown in Figure 1 represents correctly both transition mechanisms—those occuring by a saddle-node bifurcation as well as those induced by BBC, given here by the branch of saddle points. In systems with two or more dynamical variables, however, this (1 + 1)-dimensional response diagram no longer explains all possible transitions since it disregards the increased dimension and complexity of the basin boundary. For instance, the perturbation (0 → 1*p*) may result in the "unexpected" transition to 1*p*′. Conversely, the perturbation (1*p*′ → 1*p*) does not take the system to 0 but reverts it instead to 1*p*′. Apparently, the basin boundary lies within the interval (0, 1*p*). Another BBC transition (2*p* → 2*p*′) may be initiated by suddenly increasing the control parameter from 0 to 2*p*. Of course, none of these dynamics are truly unexpected if the basin boundaries are considered in the original, unreduced phase space.[7] Just as the geometry of high-dimensional objects may appear counter-intuitive when projected into a space of lower dimension,[8] related topological surprises may happen when a high-dimensional dynamical system is projected into a reduced phase space of lower dimension. For instance, the trajectories of a chaotic system appear to cross in two dimensions, an event that cannot occur in unreduced phase space.

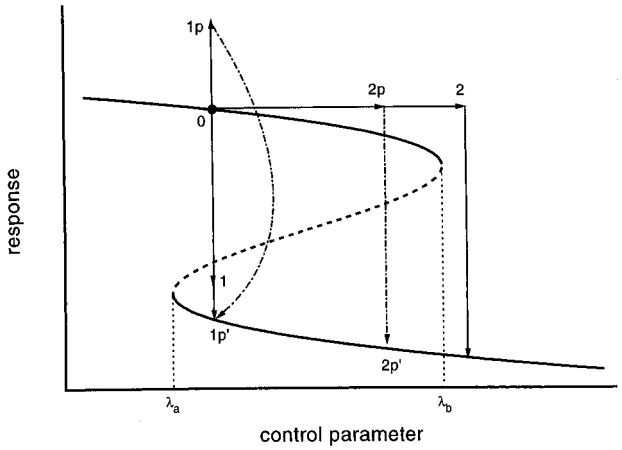

Figure 1. Schematic (1 + 1)-dimensional response diagram of a bistable system. Transitions may be induced by perturbing a dynamical variable ("response"), as in (0 → 1), or by changing the control parameter beyond the stability limit of the steady state, as in (0 → 2). BBC transitions, (1*p* → 1*p*′) and (2*p* → 2*p* ′), not anticipated by this diagram, may take place after perturbations of the dynamical variable (0 → 1*p*) and of the control parameter (0 → 2*p*), respectively.

We present here experimental evidence for the two nonadiabatic transitions just described in the bistable Belousov−Zhabotinsky system. Using a two-variable flow-Oregonator

† Permanent address: L.V. Pizarzhevskii Institute of Physical Chemistry, Ukrainian Academy of Sciences, prosp. Nauki 31, Kiev, Ukraine 252039

* Author to whom correspondence is to be addressed. E-mail: mmenzing@alchemy.chem.utoronto.ca.

⊗ Abstract published in *Advance ACS Abstracts,* August 1, 1997.

S1089-5639(97)01475-8 CCC: $14.00

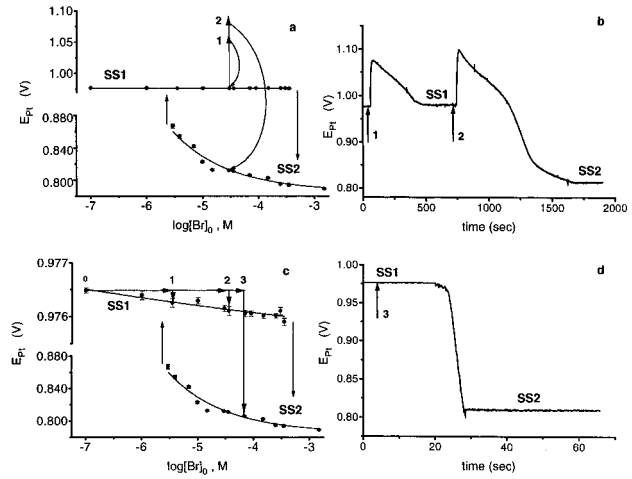

Figure 2. (a) Experimental response diagram and responses to injections of 1 M Ce(IV). The arrow 1 indicates a subcritical perturbation (1.1 mL of 1 M Ce(IV)) and in 2 a supercritical perturbation (1.3 mL of 1 M Ce(IV)). The transition is (2 → SS2). (b) Time series following perturbations 1 and 2. (c) Response to sudden jumps of the control parameter $[Br^-]_0$. The response diagram is as in (a). Starting from 0, two subcritical 1, 2 and one supercritical perturbation 3 are shown. The nonadiabatic transition is (3 → SS2). (d) Time series following perturbation 3.

model we interpret these transitions by examining the geometry of the (2 + 1)-dimensional response diagram (2 variables + 1 parameter) together with that of the basin-boundary surface. This representation allows one to assess the relative roles of deliberately induced and of noise-induced BBC transitions and of saddle-node transitions. In contrast to the saddle-node transition that may be initiated through (infinitesimally) small perturbations, BBC requires large perturbations. BBC is related, in this regard, to excitability[21] and to canard explosions.[19,20] In all of these, a manifold exists in phase space that separates two types of trajectories that evolve qualitatively differently. Our analysis shows that in the BZ system, BBC may be induced so readily because the basin boundary lies very close to the branch of initial steady states. The reason for this unique basin boundary topology is purely kinematic: it lies in the separation of time scales of a stiff dynamical system. Finally, it is possible to identify the chemical mechanism for the critical divergence of trajectories at the basin boundary. Through a numerical analysis of the rates of the elementary steps that constitute the Oregonator mechanism, it is shown that the critical divergence of trajectories at the basin boundary is due to the step that produces HOBr from $HBrO_2$ and Br^-.

2. Experiments and Results

The cylindrical plexiglass CSTR ($V = 28$ mL; thermostated at $T = 36$ °C) had a rectangular stirrer (8 × 15 mm paddle, made of Teflon-coated steel) positioned 30 *mm* above the reactor bottom.[9] The stirring rate was kept at 1500 rpm. The reactants were peristaltically pumped through two ports on opposite sides just below the stirrer blade at a constant rate of 1.99 mL/min, corresponding to the residence time $\tau_0 = 282$ s. Reagents, prepared from analytical grade chemicals, were stored in three different solutions, each of which contained 1.5 M H_2SO_4: (1) 8.1×10^{-3} M $NaBrO_3$; (2) 4.35×10^{-3} M $Ce_2(SO_4)_3$ and 0.03 M malonic acid; (3) the third solution contained NaBr of adjustable concentration, used as the control parameter. The feedstreams 2 and 3 were premixed and entered the reactor at twice the flow rate as that of feedstream 1. Experimental conditions were similar to those described elsewhere.[10] The state of the system was monitored by a 0.1 × 3 mm Pt electrode together with a $Hg/HgSO_4$ reference electrode. The impedance-matched electrode signal was fed, after digitization by an A/D converter, into a personal computer.

Three kinds of experiment were performed: In the first, the hysteresis was mapped in small steps as a function of bromide concentration in the inflow. In the second experiment, the dynamical variable [Ce(IV)] was transiently increased by rapidly injecting 1 M cerium(IV) sulfate solution into the premixed feedstream, as shown in Figure 2a,b, using a rubber septum and a microsyringe. In the third experiment, the system's response to sudden jumps of the control parameter $[Br^-]_0$ was followed, always from the same initial condition, as shown in Figure 2c,d.

Figure 2a,c shows the hysteretic adiabatic response as a function of control parameter. At low $[Br^-]_0$, the system resides

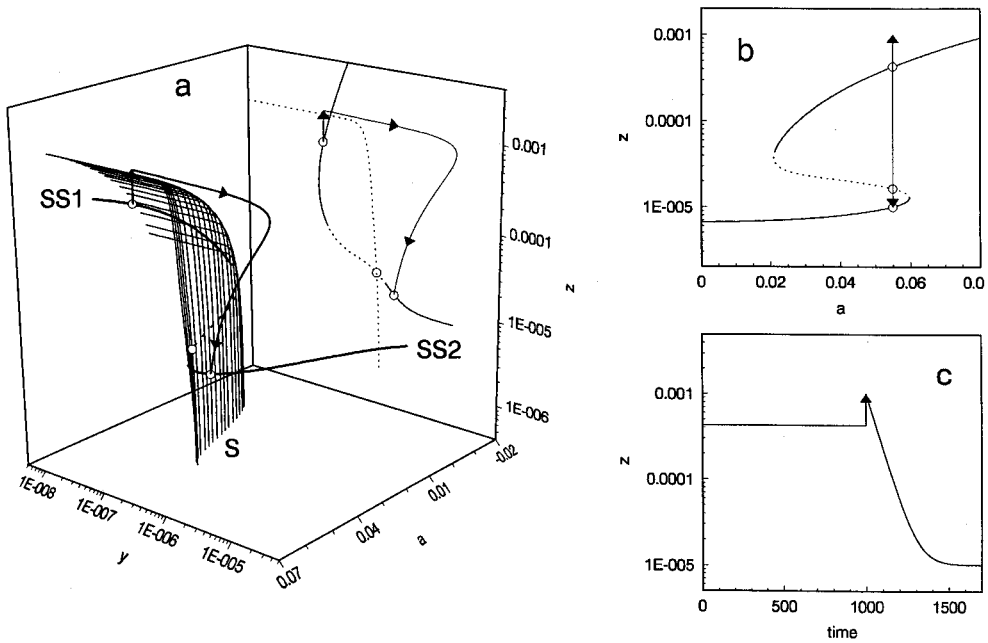

Figure 3. (a) Computed steady state manifold, separatrix surface *S*, and response to a supercritical perturbation of the dynamical variable z = [Ce(IV)]. The projection (y,z) into the phase plane is included. (b) The (a,z) projection of (a). (c) Time series response to a supercritical injection of Ce(IV).

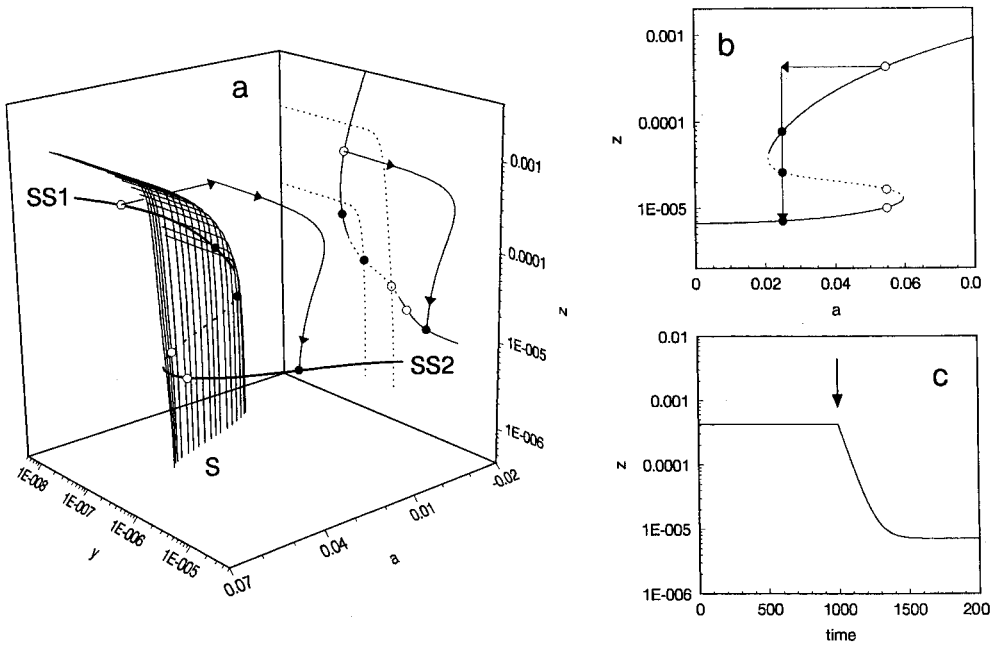

Figure 4. (a) Computed steady state manifold and separatrix surface *S* as in Figure 3. Response to a supercritical jump in feed stream concentration $a = [BrO_3^-]_0$. The projection into the phase plane, including the parameter-induced shift of the separatrix, is drawn on the side panel. (b) The (*a*,*z*) projection of (a). (c) Time series corresponding to (a).

in steady state SS1, characterized by high [Ce(IV)] and autocatalysis turned on. Beyond the upper critical bromide concentration $C_1 = 4 \times 10^4$ M, the system switches to the second, low [Ce(IV)] steady state SS2. When the $[Br^-]_0$ scan is reversed, transition to SS1 occurs at the lower hysteresis limit $C_2 = 2.8 \times 10^6$ M. The upper, autocatalytic state SS1 is sensitive to BBC as discussed below. It depends only weakly on control parameter, while the unreactive, lower SS2 shows pronounced parameter dependence and curvature.

To obtain the hysteresis limits, the bifurcation parameter was changed in steps $\Delta[Br^-]_0$ of decreasing magnitude. We found that the lower hysteresis limit C_2 is independent of step size. In contrast, the value of the hysteresis limit C_1 of the upper branch SS1 is highly sensitive to $\Delta[Br^-]_0$. To document this phenomenon, the Br^- feed was suddenly switched from the same initial state on SS1 at ($[Br^-]_0 = 10^{-7}$M) by replacing the feed stock with a new solution of higher concentration, as indicated by the horizontal arrows in Figure 2c. If the perturbation $\Delta[Br^-]_0$ is sufficiently small, the system remains in SS1. Arrows 1 and 2 indicate this kind of response. Above a critical value of $\Delta[Br^-]_0$, which is, however, small enough for the hysteresis limit C_1 not to be exceeded, the system no longer relaxes to SS1 but eventually transits to SS2 as indicated by arrow 3 in Figure 2c. Figure 2d is the corresponding time series of the electrode response.

The sensitivity of SS1 to perturbations of the dynamical variable [Ce(IV)] is illustrated in Figure 2a,b. For sufficiently small injected amounts of Ce(IV), the system reverts to SS1 as indicated by the arrow labeled 1 in Figure 2a and the initial portion of Figure 2b. For perturbations greater than 1.1 mL of 1 M Ce(IV) injected solution, as indicated by the arrow labeled 2, the system transits to SS2. In both transitions considered here, the basin boundary is apparently crossed. Its geometry will be calculated in the next section.

3. Interpretation and Discussion

3.1. Model. The two types of transitions observed in experiments may be illustrated by the two-dimensional version of the Oregonator model. This model, proposed by Field and Noyes[22] as a skeleton model of the Belusov−Zhabotinsky reaction, consists of the following steps:

$$BrO_3^- + Br^- + 2H^+ \xrightarrow{k_1} HBrO_2 + HOBr$$

$$HBrO_2 + Br^- + H^+ \xrightarrow{k_2} 2HOBr$$

$$BrO_3^- + HBrO_2 + 2Ce(III) + 3H^+ \xrightarrow{k_3} 2HBrO_2 + 2Ce(IV) + H_2O \quad (1)$$

$$2HBrO_2 \xrightarrow{k_4} BrO_3^- + HOBr$$

$$BrMA + Ce(IV) \xrightarrow{k_5} {}^1/_2 f\, Br^- + Ce(III)$$

In a continuously stirred tank reactor, this mechanism may be reduced to the following two-dimensional model

$$dy/dt = -k_1 a h^2 y - k_2 h x y + k_5 f b z + k_0(y_0 - y) \quad (2)$$

$$dz/dt = 2k_3 a h x - k_5 b z + k_0(z_0 - z)$$

where x is given through adiabatic elimination by:

$$x = \frac{1}{4k_4}\Big\{ -2k_2 h y + k_3 h a - k_0 + \sqrt{(k_3 h a - k_2 h y - k_0)^2 + 8k_1 k_4 h^2 a y}\Big\} \quad (3)$$

Here $x \equiv [HBrO_2]$, $y \equiv [Br^-]$, $z \equiv [Ce(IV)]$, $h \equiv [H^+]$, $a \equiv [BrO_3^-]$, $b \equiv [MA]$; $y_0 \equiv [Br^-]_0$, $z_0 \equiv [Ce(IV)]_0$ and k_0 is the inverse residence time. The rate constants and parameter values are $k_1 = 2.0\ M^{-3}\ s^{-1}$, $k_2 = 2.0 \times 10^8\ M^{-2}\ s^{-1}$, $k_3 = 2.0 \times 10^3\ M^{-2}\ s^{-1}$, $k_4 = 4.0 \times 10^8\ M^{-1}\ s^{-1}$, $k_5 = 1.0\ M^{-1}\ s^{-1}$, $h = 0.5$ M, $b = 0.005$ M, $y_0 = 1 \times 10^{-5}$ M, $z_0 = 1 \times 10^{-5}$ M, $f = 0.2$, $k_0 = 0.01\ s^{-1}$. Notice that the acidity, h, and malonic acid concentration, b, are retained explicitly in the rate equations.

The bromate concentration a was chosen as the control parameter. The steady state manifold was obtained by numerical

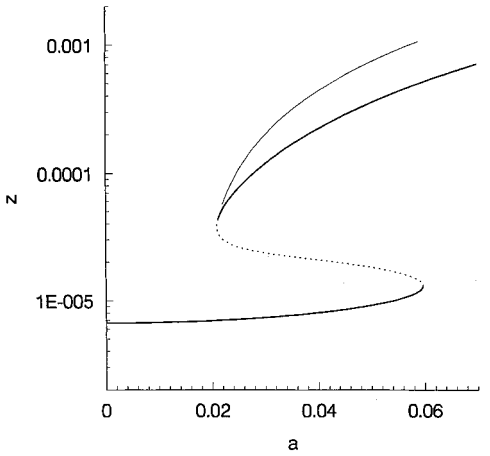

Figure 5. Response diagram showing the distance of the basin-boundary surface in the *z* direction.

continuation. The separatrix was calculated at fixed values of *a* as the inset of the unstable steady state (saddle point) by integrating the model with reversed time, starting close to the saddle point. The separatrix surface S in the combined phase and control space was obtained by repeating this calculation for a range of *a*. The responses to the perturbations applied to *a* and to *z* were also obtained by numerical integration.

3.2. Results. Figure 3a and 4a offer different views of the same steady state manifold and separatrix surface S. Figure 3a illustrates the response to perturbation of the dynamical variable *z*, and Figure 4a to perturbation of the control parameter *a*. The vertical lines that make up the surface S are the separatrices calculated at constant values of *a*. On the upper branch SS1 of stable steady states (solid lines) at high *z* and low *y*, autocatalysis is switched on; on the other, lower branch SS2, autocatalysis is off. The branch of unstable steady states (saddle points, shown by dashed line) lies in the separatrix surface, while the stable branches begin to diverge from this surface at the two saddle-node points. The projections into the (*y*,*z*) and (*a*,*z*) planes are the traditional phase and response diagrams.

It should be noted that the separatrix surface S is vertical at the branch of unstable steady states, but it bends into the direction of the *y* axis at high values of *z*. Beyond the upper saddle-node point, this surface tends to hug the upper SS1 branch and to diverge from it only gradually. To illustrate this, Figure 5 shows the shortest vertical distance from the upper SS1 branch to the separatrix surface. Accordingly, the shortest distance from any steady state on the upper branch to the separatrix surface is less than the distances to either the corresponding saddle-node point or to the saddle point. Hence the separatrix may be reached relatively easily through perturbations that are smaller in magnitude than those required in the corresponding one-variable system.

Figure 3a illustrates the response to a perturbation of the *z* variable at fixed *a*, indicated by the vertical arrow, starting from the open circle. A sufficiently large perturbation crosses the separatrix, and the system relaxes to the coexisting SS2, as indicated by the trajectory. The projection into the phase plane (*y*,*z*) shows the steady states and the separatrix together with the perturbation and the response trajectory. The projection into the (*z*,*a*) plane represents the "unexpected" response mentioned in the Introduction. The full response diagram, Figure 3a, and its projection into the phase plane, Figure 3b, including the trajectory shown, resolve the apparent paradox. Figure 3c shows the corresponding time series of relaxation to the competing attractor. The response is similar to that observed in experiment, Figure 2a,b.

Figure 4a illustrates the response of the same system to a sudden and persistent parameter change that is large enough to cross the separatrix, but too small to cause a saddle-node transition. The steady states before and after the parameter change are marked by the open and solid circles, respectively. The sudden perturbation lifts the system away from the SS1 manifold along the horizontal arrow and, in doing so, crosses the separatrix surface. Then the system relaxes to the competing SS2 (solid circle) at the new parameter value. The corresponding time series for a supercritical parameter jump is shown in Figure 4b and should be compared with the experimental result, Figure 2d. The projection into the phase plane illustrates the steady states at the old (open circles) and new (open circles) parameter values, together with the old and new separatrices: the parametric perturbation redraws the basin boundary such that the old, unperturbed phase point falls now into the basin of attraction of the competing SS2 (solid circle) on the lower branch. Again, the projection into the (*a*,*z*) plane gives the unexpected responses of Figures 1 and 2a. In general, the critical value of the perturbation depends on the rate with which the perturbation is applied.

3.3. Discussion. We have demonstrated experimentally and computationally two types of basin-boundary transitions that may result from large, sudden changes of a dynamical variable on the one hand or of a control parameter on the other hand. In general, the critical value of a perturbation depends on the rate with which the perturbation is applied.[23] In addition to drawing the attention of experimentalists to the importance of choosing a sufficiently small step size in the determination of bifurcation diagrams and to the shortcomings of (1 + 1)-dimensional response diagrams, the three further aims are presently: to explain the close relationship of BBC transitions to the phenomena of excitability and canard explosions,[19,20] to explain why such transitions are more likely in stiff systems with widely separated time scales, and finally to determine the reaction step that plays the key role in triggering the basin-boundary transitions.

The bistability transition induced by a sudden, nonadiabatic change of control parameter results from basin-boundary crossing and is closely related to excitability and canard explosions. In all these phenomena there exists a threshold or boundary in phase space such that trajectories, starting arbitrarily close but on opposite sides of it, evolve in qualitatively different ways. In the case of excitability,[20,21] a subcritical perturbation results in a trajectory that smoothly returns the system to its starting point, whereas a supercritical perturbation results in a large excursion in phase space before eventually returning the system to its steady state. In canards, small amplitude oscillations are transformed into large relaxation oscillations when the small limit cycle crosses a locus of points where the curvature of trajectories is zero.[19,20]

Although BBC transitions are not restricted to stiff dynamical systems, they are more likely to occur in such systems. To illustrate the relationship between stiffness and the geometry of basin boundaries, consider the classical Bonhoeffer−van der Pol system,[13] whose equations and parameters values are given in the caption of Figure 6. Changing the time scale parameter ϵ changes neither the nullclines nor the values of the steady state concentrations. However, for small values of ϵ, *x* changes faster than *z* and the trajectories are therefore nearly parallel to the *x* -axis, except on the S-shaped *x* nullcline. Hence, at $\epsilon \ll 1$, the inset of the saddle point (the basin boundary) also bends in the direction of the fast *x* variable. This is shown in Figure 6. Consequently, for $\epsilon \ll 1$ the threshold for basin-boundary

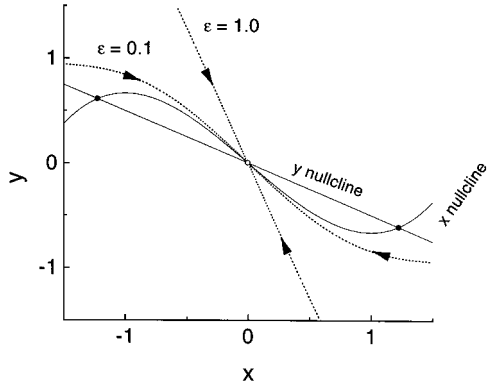

Figure 6. Phase portrait for the Bonhoeffer−van der Pol system: $\dot{x} = 1/\epsilon(x - (x^3/3) + y)$, $\dot{y} = b - x - cy$. Parameter values are $c = 2.0$, $b = 0.1$. The dotted lines are the basin boundaries for two different values of ϵ. Note how the basin boundary appoaches the steady states at the lower value of ϵ.

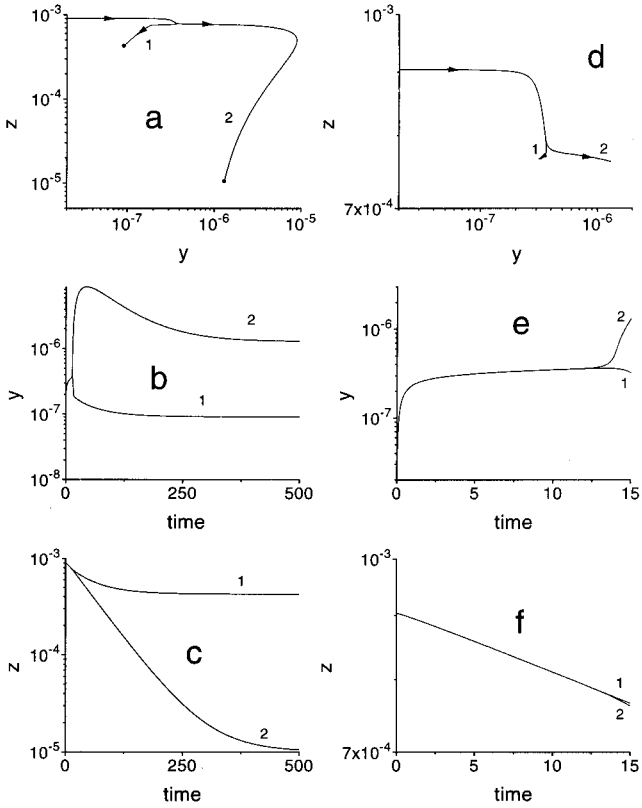

Figure 7. (a) Divergence of two trajectories (labeled 1 and 2) starting arbitrarily close to but on opposite sides of the basin boundary for system 2. $a = 0.055$. The full dots are the asymptotic steady states. (b, c) time evolution of the variables y, z along the two trajectories. (d, e, f) show the initial divergence of (a, b, c) in greater detail.

transitions becomes smaller, and relatively small parameter changes may lead to the transitions of the type shown in Figure 4.

The gradual convergence of the stable SS1 manifold and the separatrix at the saddle-node point for the Oregonator model, as shown in Figure 5, makes noise-induced transitions very likely in the neighborhood of the saddle-node point. Hence, in the presence of external noise, noise-induced transitions will occur in proportion to the noise level and the reduced threshold values, preventing the system from ever reaching the adiabatic saddle-node point predicted by the (1 + 1)-d response diagram, Figure 1. In retrospect it is therefore not surprising that the search for critical growth of fluctuations, anticipated near the bistability limit of the chlorite/iodide reaction was not successful.[14] The type of facile, noise-induced BBC transition discussed here lends further support to the earlier explanation[15] of the effect of stirring on the attributes of limit cycle oscillations: it is often observed that the oscillation amplitude and period decrease when an oscillating system is stirred more slowly and becomes more inhomogeneous.[15,16] It was argued[15] that noise-induced perturbations similar to the ones considered here for bistable systems will cause the limit cycle to contract and oscillations to accelerate.

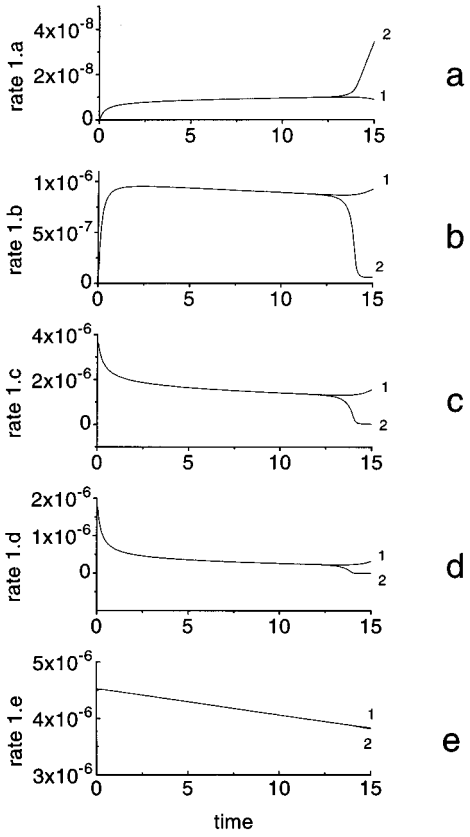

Figure 8. Rates of the five steps in scheme 1 along the two trajectories shown in Figure 7.

To conclude this Discussion, we examine the chemical basis of the divergence of trajectories that start arbitrarily close to, but on opposits sides of, a basin boundary. Figure 7 illustrates the evolution of two such trajectories. They start at (y_1,z_1) and (y_2,z_2) where $y_1 = y_2$ and $z_1 = z_2 + 10^{-8}$. The three left panels are the phase portrait (panel a) and time evolution of the variables y (panel b) and z (panel c) of the trajectories from their initial conditions to the final states. The right-hand panels d, e, f illustrate the evolution of the two adjacent trajectories up to a point where they suddenly begin to diverge. The key question, at this point, is: which chemical step in mechanism 1 is responsible for this critical divergence?

Figure 7e,f shows that the values of z diverge much less than those of y—hence the clue to the divergence must be sought in the evolution of y. The reason why initially the variable z diverges very little can be understood by examining the rates of the two steps 1c and 1e (Figure 8c,e), which contribute to the rate of change of z. The rate of step 1e is twice as large as that of 1c, but its value does not diverge significantly. The rate of change of $y = [Br^-]$ is governed by steps 1a, 1b, and 1e. Among these three steps, 1e may be discounted since the divergence in its rate is small (Figure 8e). Similarly, step 1a may be neglected since the absolute magnitude of its rate is 1 order of magnitude less than that of 1b. Hence, we conclude that the reaction step 1b (i.e. the production of HOBr from

$HBrO_3$ and Br^-) is the key step that triggers the divergence of trajectories near the unstable manifold.

Acknowledgment. This work was supported by NSERC.

References and Notes

(1) Thompson, J. M. T.; Soliman M. S. *Proc. R. Soc. London* **1990**, *A428*, 1.
(2) Pifer, T.; Ganapathisubhramanian, N.; Showalter, K. *J. Chem. Phys.* **1985**, *83*, 1101.
(3) Gray, P.; Scott, S. C. *Chemical Oscillations and Instabilities*; (Oxford University Press: Oxford, 1994.
(4) Maselko, J. *Chem. Phys.* **1982**, *67*, 17.
(5) Celarier, E.; Kapral, R. *J. Chem. Phys.* **1987**, *86*, 3357.
(6) Grebogi, C.; Ott, E.; Yorke, J. A. *Physica* **1987**, *24D*, 243.
(7) Bar-Eli, K.; Geiseler, W. *J. Phys. Chem.* **1983**, *87*, 1352.
(8) Abbott, B. *Flatland*; Dover: New York, 1952.
(9) Dutt, A. K.; Menzinger, M. *J. Phys. Chem.* **1990**, *94*, 4867. Ali, F.; Menzinger, M. *J. Phys. Chem.* **1991**, *95*, 6408.
(10) DeKepper, P.; Boissonade, J. *J. Chem. Phys.* **1981**, *75*, 189.
(11) Bar-Eli, K.; Noyes, R. M. *J. Chem. Phys.* **1987**, *86*, 1927.
(12) Gaspar, V.; Showalter, K. *J. Chem. Phys.* **1988**, *88*, 778.
(13) Koper, M. T. M. *J. Chem. Phys.* **1995**, *102*, 5278.
(14) Menzinger, M.; Dutt, A. K. *J. Phys. Chem.* **1990**, *94*, 4510.
(15) Menzinger, M.; Jankowski, P. *J. Phys. Chem.* **1986**, *90*, 1217.
(16) Menzinger, M.; Jankowski, P. *J. Phys. chem.* **1990**, *94*, 4123.
(17) Menzinger, M.; Boukalouch, M.; DeKepper, P.; Boissonade J.; Roux, J. C.; Saadaoui, H. *J. Phys. Chem.* **1986**, *90*, 313.
(18) Grebogi, C.; Ott, E.; Yorke, J. A. *Phys. Rev. Lett.* **1983**, *50*, 935.
(19) Peng, P.; Gaspar, V.; Showalter, K. *Philos. Trans. R. Soc. A* **1991**, *337*, 275.
(20) Bar-Eli, K.; Brons, M. *J. Phys. Chem.* **1991**, *95*, 8706.
(21) Noszticzius, Z.; Wittmann, M.; Stirling, P. *J. Chem. Phys.* **1987**, *86*, 1922.
(22) Field, R. J.; Noyes, R. M. *J. Chem. Phys.* **1974**, *60*, 1877.
(23) Erneux, T.; Laplante, J. P. *J. Chem. Phys.* **1989**, *90*, 6129.